

Self-Supervised Point Cloud Representation Learning with Occlusion Auto-Encoder

Junsheng Zhou^{1,*}, Xin Wen^{1,2,*}, Yu-Shen Liu^{1**}, Yi Fang³, and Zhizhong Han⁴

¹ School of Software, BNRist, Tsinghua University, Beijing, China

² JD Logistics, JD.com, Beijing, China

³ New York University, New York, USA

⁴ Department of Computer Science, Wayne State University, Detroit, USA

Abstract. Learning representations for point clouds is an important task in 3D computer vision, especially without manually annotated supervision. Previous methods usually take the common aid from auto-encoders to establish the self-supervision by reconstructing the input itself. However, the existing self-reconstruction based auto-encoders merely focus on the global shapes, and ignore the hierarchical context between the local and global geometries, which is a crucial supervision for 3D representation learning. To resolve this issue, we present a novel self-supervised point cloud representation learning framework, named 3D Occlusion Auto-Encoder (3D-OAE). Our key idea is to randomly occlude some local patches of the input point cloud and establish the supervision via recovering the occluded patches using the remaining visible ones. Specifically, we design an encoder for learning the features of visible local patches, and a decoder for leveraging these features to predict the occluded patches. In contrast with previous methods, our 3D-OAE can remove a large proportion of patches and predict them only with a small number of visible patches, which enable us to significantly accelerate training and yield a nontrivial self-supervisory performance. The trained encoder can be further transferred to various downstream tasks. We demonstrate our superior performances over the state-of-the-art methods in different discriminant and generative applications under widely used benchmarks. Our code will be available at <https://github.com/junshengzhou/3D-OAE>.

Keywords: 3D representation learning, Self-supervised learning.

1 Introduction

Point cloud plays a crucial role in 3D computer vision applications [8,2,30] due to its flexibility to represent arbitrary geometries and memory-efficiency. In this paper, we specifically focus on the task of learning representations of point clouds

* Equal contribution.

** Corresponding author.

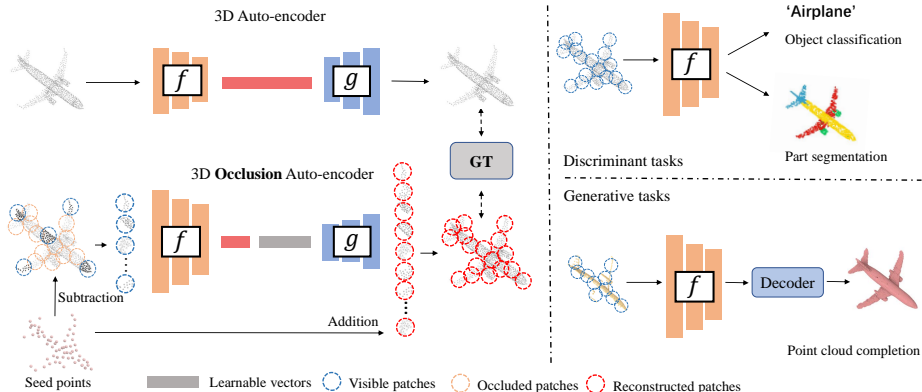


Fig. 1. Comparison between previous auto-encoders and our 3D-OAE. The f and g indicate the encoder and decoder of an auto-encoder. The seed points is extracted from the original shape using FPS. Unlike other auto-encoders which takes the whole shape as input to reconstruct itself, 3D-OAE randomly occludes a high ratio of patches, encodes only on the visible patches, and learns to recover the complete shape. After self-supervised learning, we keep f for further fine-tuning. We demonstrate that the f learned by 3D-OAE shows powerful performances in both discriminate tasks (eg. object classification, part segmentation) and generative tasks (eg. point cloud completion).

without manually annotated supervision. As 2D images, learning representations for 3D point clouds has been comprehensively studied for many years, and the research line along the 2D and 3D representation learning shares a lot of common practices, such as the auto-encoder based framework and the self-reconstruction based supervision. The recent development in both NLP and 2D computer vision fields has also driven several improvements in 3D representation learning, such as PCT [14], Point-BERT [64] and STRL [20]. However, the different data characteristics between the 2D and 3D domains limit the direct applications of many 2D improvements into 3D scenarios, e.g. the differences between ordered 2D grids and the unordered 3D points.

One of the major challenges is to learn the hierarchical context between the global structure and local geometries. In 3D scenarios, this is more difficult than the learning of 2D images due to the discrete nature of 3D points. In most previous methods, the 3D auto-encoder usually relies on the self-reconstruction as the supervision to focus on the global structures and the local shapes. However, the simple self-reconstruction based framework usually do not explicitly distinguish the local shapes and the global structures apart. As a result, both of them are only revealed by the shape matching constraints (e.g. Chamfer Distance) as a whole, while more detailed self-supervision to reveal the local to global hierarchy in 3D point clouds is merely discussed.

The recent improvements of mask-based 2D auto-encoders [17] has been proved to be effective in image representation learning through the inference of the overall image information based on the visible local patches. It provides a new perspective to establish the self-supervision between the local and global



Fig. 2. Visualization of reconstructing shapes from seed points and visible patches. We show the reconstructing results of objects from different categories in the ShapeNet dataset, even including some very complex objects(eg. Motorcycle). Our model is able to reconstruct the complete shape from a highly sparse seed point cloud which has only 64 points and a highly occluded(only 25% visible) input point cloud.

information. However, due to the discrete nature of point clouds, it’s difficult to directly use 2D mask-based auto-encoder to learn 3D representations. Driven by above analysis, we present 3D-OAE, a novel Transformer-based self-supervised learning framework with Occlusion Auto-Encoder. As shown in Fig. 1, we separate the unlabelled point cloud into local point patches and centralize them to their corresponding seed points. After that, we occlude a large proportion of the patches but remain the seed points, and learn to recover occluded patches from seed points and the visible patches. The seed points serve as global hints to guide the shape generation and the model will be forced to focus on learning the local geometries details. Specifically, we design an encoder to learn features only on the visible subset of patches, and a decoder to leverage the features of visible patches to predict the local features of the occluded ones, and finally reconstruct the occluded patches with seed points as the global hints. After self-supervised learning without any manual annotation, we can transfer the trained encoder to different downstream tasks. We demonstrate our superior performances by comparing our method under widely used benchmarks.

Our main contributions can be summarized as follows:

- We proposed a novel self-supervised learning framework named 3D Occlusion Auto-Encoder. Unlike previous 3D auto-encoders, 3D-OAE designs an asymmetrical encoder-decoder Transformer architecture to learn the patterns from the visible local patches and leverage them to control the local geometry generation of the occluded patches. After self-supervised learning, the trained encoder can be transferred to new downstream tasks.
- Our 3D-OAE can remove a large proportion(eg. 75%) of point cloud patches before training and only encodes a small number of visible patches. This enable us to accelerate training for 3-4 times and makes it possible to do self-supervised learning in large scale unlabelled data efficiently.
- We achieved the state-of-the-art performances in six different downstream applications compared with previous self-supervised methods.

2 Related Work

Representation Learning on Point Clouds Different from structured data like images, point clouds are unordered sets of vectors, which brings great challenges to the learning of representations. Qi et al. [32] pioneered point cloud learning by purposing PointNet, which directly input the raw point cloud into point-wised MLPs and use max-pooling to solve the permutation invariant of point cloud. Further more, PointNet++ [33] applies query ball grouping and hierarchical spatial structure to increase the sensitivity to local geometries. Some works followed this idea and developed different grouping strategies [54,60,18]. A number of approaches build graphs to connect points and aggregate information through graph edges [51,12,47,39,49]. DGCNN [51] propose to use graph convolutions on KNN graph nodes, and GACNet [49] apply attention mechanism in graph convolutions. Some other methods purpose to use continuous convolutions on point clouds [19,59,70,40,24,54,43]. PointCNN [24] applies convolution neural network on point set after reordering points with special operators.

Inspired by the great success achieved by the Transformers in both NLP [46,9,21,26,34,4] and 2D vision [22,7,5,27,10,3], some recently works try to apply Transformers in 3D point cloud representation learning [71,14,63]. Zhao et al. [71] propose to use vectorized self-attention mechanism in Transformer-layer, and apply a hierarchical structure with local feature aggregation. Guo et al. [14] propose to use neighbour embedding to enhance the representation learning ability. However, previous Transformer-based methods on point cloud representation learning bring in inevitable inductive biases and manual assumptions, the standard Transformer with no inductive bias is proved to perform poorly [64] due to the limited scale of point cloud data. In this work, we aim to extend the success of standard Transformer to point cloud representation learning.

Self-supervised Learning on Point Clouds Self-supervised learning (SSL) is to learn the representation from unlabelled data, where the supervision signals are built from the data itself. Since the annotation of point clouds is often time-consuming and error-prone, the performance of supervised approaches is difficult to be further improved. Therefore, SSL on point clouds becomes more and more important. Recently, several works propose to use SSL techniques for point cloud representation learning [61,58,48,41,37,36,35,23,11,69]. Sauder et al. [37] propose to rearrange shape parts and reconstruct the original shapes. PointContrast [58] design a SSL scheme by contrastive learning on different views of point clouds. Inspired by BERT, Point-BERT [64] achieves great performance by pre-training a standard Transformer in a BERT-style SSL scheme. However, Point-BERT only focuses on distinguishing tokens of different patches, makes it difficult for them to transfer to downstream generative tasks.

Auto-encoder. An auto-encoder architecture consists of two parts: an encoder and a decoder. A number of approaches [48,61,11,16,25] apply auto-encoder architecture to learn meaningful representations from unlabelled point clouds. The purpose of point cloud auto-encoder is to learn the presentation from the input shape and then reconstruct the shape from the learned low-dimension latent

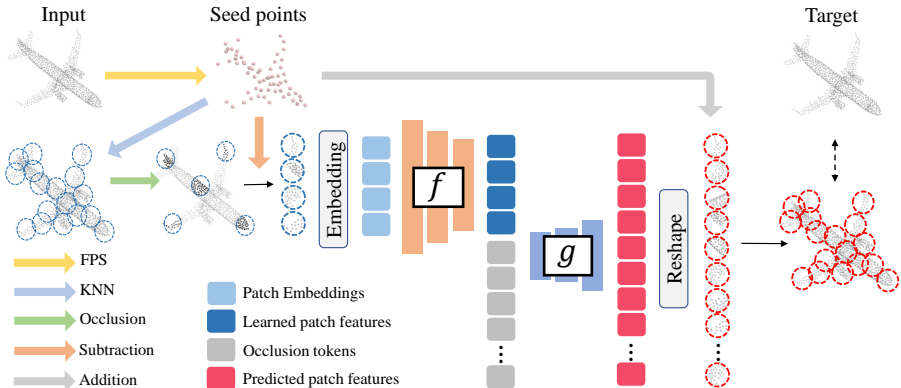


Fig. 3. Overview of 3D-OAE. The f and g indicate standard Transformer-based encoder and decoder. We first extract seed points from the input point cloud using FPS, and then separate the input into point patches by grouping local points around each seed point using KNN. After that, we randomly occlude high ratio of patches and subtract each visible patch to its corresponding seed point for detaching the patch from its spatial location. The encoder f operates only on the embeddings of visible patches and the learnable occlusion tokens are combined to the latent feature before decoder g . Finally, we operate addition to the output patches and their corresponding seed points to regain their spatial locations and further merge the local patches into a complete shape, where we compute loss function with the ground truth.

code. FoldingNet [61] designs a point cloud auto-encoding with a folding-based decoder. OcCo [48] proposes to complete view-occluded point cloud with a standard point cloud completion network. However, these methods only focus on the generation ability of the whole shape, thus mixing the local and global geometry features together, making it hard to transfer the knowledge to downstream tasks. Recently, in 2D vision, He et al. [17] propose a new form of auto-encoders named MAE by masking regular patches of images and learning to recover the masked parts. Partly inspired by MAE, we design a new self-supervised learning framework to recover the complete shapes from the highly occluded shapes.

3 Occlusion Auto-encoder

The overall architecture of 3D-OAE is shown in Fig. 3. Like other point cloud auto-encoders, 3D-OAE consists of an encoder which learns the representation from the input shape and a decoder to reconstruct the original shape from the learned representation. Unlike other point cloud auto-encoders which operates on the whole shape, 3D-OAE divides the complete shape into groups of patches, highly occludes them, and learns to recover the missing patches of shapes. To achieve this, an asymmetrical encoder-decoder architecture is designed with an encoder only operates on the visible subset of patches, and a decoder to predict local features of occluded patches from the visible ones. After that, we combine

the predicted local features of occluded patches and their corresponding seed points which serve as global hints to infer the missing geometries that semantically match the input 3D shape. After self-supervised learning, we can leverage the encoder in different downstream tasks as illustrated in Fig. 1. Specifically, we first operate average pooling to aggregate all local features extracted from the trained encoder into a global feature for representing the whole shape, and then fed it into the special decoders of different downstream tasks.

3.1 Grouping and Occluding

Previous Transformer-based methods treat each single point in the original shape as a minimum operation unit like words in sentences. However, it brings huge computational complexity and large demand for memory due to the large scale of point cloud data (we don't expect a sentence to have thousands of words). Inspired by previous works [10,64], we choose to use patches of point clouds as the minimum unit. To achieve this, we first use Furthest Point Sampling (FPS) to sample seed points $s \in \mathbb{R}^{M \times 3}$ on a given input point cloud $p \in \mathbb{R}^{N \times 3}$, and then use K Nearest-Neighbour (KNN) to sample sets of point patches $\{g_i | g_i \in \mathbb{R}^{G \times 3}\}$ around each seed point $\{s_i\}_{i=1}^M$, as shown in Fig. 3. But it doesn't work to put these patches directly into a neural network because the structure information and spatial coordinates are entangled in point clouds. We solve this problem by centralizing each patch to its corresponding seed point, thus each patch only contains its local geometry details while seed points provide the global hints.

We apply a straightforward occluding strategy: we randomly select a subset of seed points $\{s_i\}_{i=1}^R$, and then remove their corresponding patches $\{g_i\}_{i=1}^R$. After that, we project each of the remain visible patches $\{g_i\}_{i=1}^{M-R}$ into a patch embedding as shown in Fig. 3 using a simple PointNet as:

$$E_i = \text{Max}(x_i) \in \mathbb{R}^{1 \times C}, \text{ where } x_i = \phi(g_i | \theta) \in \mathbb{R}^{G \times C}, \quad (1)$$

where ϕ and θ denotes the MLP layers and the weights, C is the channel of patch embeddings and Max denotes Max-Pooling operation. The patch embeddings $\{E_i\}_{i=1}^{M-R}$ will serve as the inputs to the encoder f .

We choose to occlude a very large regions (75%) of the original shape, more numerical comparison of occlusion ratios can be found in Table 8. Removing a high ratio of patches largely increases the difficulty of auto-encoding reconstruction, thus force model to learn a powerful representation to generate more detailed local geometries. More importantly, the design of highly occlusion strategy makes it possible for efficient self-supervised learning on large scale unlabelled point cloud data.

3.2 Auto-encoder Architecture

3D-OAE Encoder We adopt the 3D point cloud standard Transformers with multi-headed self-attention layers and FFN blocks achieved by Point-BERT [64] as unified backbone of our architecture. Specifically, our encoder is a standard

Transformer but applies only on visible patches. For the input visible patches, we first extract their patch embeddings as described in Eq. (1). To distinguish centralized patches apart, we use a simple MLP γ to extract the position embeddings of visible seed points $\{s_i\}_{i=1}^{M-R}$ and add them to their corresponding patch embeddings as:

$$\mathbb{E}_i \leftarrow \gamma(s_i|\theta) + E_i, \quad (2)$$

After that, a series of Transformer blocks is applied to these patch embeddings to learn representations. Since we use a very high occlusion ratio, the encoder operates only on a small subset (eg. 25%) of patches, which makes it possible to do self-supervised learning in very large scale unlabelled data with a relatively huge encoder.

3D-OAE Decoder The input of 3D-OAE decoder is a full set of patch embeddings consisting of the encoded visible patch embeddings and the occlusion tokens $\{T_i\}_{i=1}^R$. Each occlusion token is a learnable vector which aims at learning to reconstruct one occluded patch, and the parameters are shared among occlusion tokens. We further add the position embeddings $\{\gamma(s_i|\theta)\}_{i=1}^M$ to the full set of patch embeddings for providing the location information to the occlusion tokens. Then a stack of light-weighted Transformer blocks are further applied to learn the occlusion tokens from features of visible patches via self-attention mechanism. Since we calculate the attention map of each patch embedding to all of the others, the model will have no sensitivity about the ordering of patches, which indicates that 3D-OAE is suitable for the unordered point cloud data.

The decoder g is only used during self-supervised learning to recover the occluded parts of the original shape, only the learned encoder f is used when transferring to downstream tasks (eg. object classification, point cloud completion), which means we don't care much about the learning ability of the decoder. Therefore, we design a light-weighted decoder with only about 20% computation of the encoder. And the training process is largely accelerated since the full set of patch embeddings is only processed by the light-weighted decoder.

3.3 Optimization Objective

During training, the goal of 3D-OAE is to reconstruct the complete shape from seed points and visible point patches. After encoding and decoding, 3D-OAE outputs patch-wised vectors where each vector contains the local geometry information of a single patch. The feature channel of decoder is set to be the product of point dimensions and patch point numbers, thus each vector can be directly reshaped to the size of a local patch. Finally, the seed points are added to their corresponding patches to reconstruct the complete shape. We choose Chamfer Distance described by Eq. (3) as our loss function. Similar to BERT [9] and MAE [17], we don't pay much attention to the reconstruction ability of visible parts, and only compute loss between the points of predicted patches \mathcal{P}^o and the ground truth point cloud of these occluded patches denoted as \mathcal{P}^t .

$$\mathcal{L}_{CD}(\mathcal{P}^o, \mathcal{P}^t) = \frac{1}{2N} \sum_{\mathbf{p}^o \in \mathcal{P}^o} \min_{\mathbf{p}^t \in \mathcal{P}^t} \|\mathbf{p}^o - \mathbf{p}^t\|_2 + \frac{1}{2N} \sum_{\mathbf{p}^t \in \mathcal{P}^t} \min_{\mathbf{p}^o \in \mathcal{P}^o} \|\mathbf{p}^t - \mathbf{p}^o\|_2. \quad (3)$$

We also try to use Earth Mover’s Distance as the loss function but find it unhelpful, please see the numerical comparison in Table 7.

4 Experiments and Applications

In this section, we first introduce the self-supervised learning setting of 3D-OAE in Sec. 4.1. Next, we evaluate the proposed model with various downstream tasks in Sec. 4.2 - Sec. 4.6, including shape understanding, few-shot learning, part segmentation and transfer learning to generative tasks and real world tasks. We also conduct an ablation study in Sec. 4.7.

4.1 Self-supervised Learning

Dataset. We learn the self-supervised representation model from the ShapeNet[6] dataset which contains 57,448 synthetic models from 55 categories. We sample 1024 points from each 3D model and divide them into 64 point cloud patches using Furthest Point Sample(FPS) and K-Nearest Neighbor(KNN), where each patch contains 32 points. During training, we apply the same data augmentations as PointNet++ [33].

Training setups. In the self-supervised learning stage, we set the Transformer depth of both encoder and decoder to 12 and the number of Transformer heads both to 6. The feature channel dimension of encoder and decoder Transformers are set to 384 and 96, and the occlusion ratio is set to 75%. We adopt an AdamW [28] optimizer, using an initial learning rate of 0.0005 and a weight decay of 0.05. And we train our model for 300 epochs with a batch size of 256 on one 2080Ti.

4.2 Shape Understanding

We follow prior works [61,16,72] to evaluate the shape understanding capability of our self-supervision model using the ModelNet40 [55] benchmark. After training our models in ShapeNet [6] as detailed in Sec. 4.1, we evaluate the learned representation of trained encoder in the following experiments.

Linear SVM In this experiment, we train a linear Support Vector Machine(SVM) classifier using the representation from our trained encoder Transformer. The number of point clouds is down-sampled to 2048 for both training and testing. The comparison of classification results is shown in Table 1. Our proposed 3D-OAE achieves state-of-the-art performance of 92.3% accuracy on test sets, while the runner-up method only achieves 91.2% accuracy. It’s worth noting that this result has reached the accuracy of train a classification network from scratch(eg. PointNet++(90.5%), DGCNN(92.2%)), which proves that the representation domain learned by 3D-OAE is highly decoupled.

Table 1. Linear evaluation for shape classification on ModelNet40. A linear classifier is trained on the representation learned from the ShapeNet dataset by different self-supervision methods. STransformer means 3D standard Transformer.

Method	Input	Accuracy
3D-GAN[53]	voxel	83.3%
VIP-GAN[15]	views	90.2%
Latent-GAN[45]	points	85.7%
SO-Net[23]	points	87.3%
FoldingNet[61]	points	88.4%
MRTNet[12]	points	86.4%
3D-PointCapsNet[72]	points	88.9%
MAP-VAE[16]	points	88.4%
PointNet + Jiasaw[37]	points	87.3%
DGCNN + Jiasaw[37]	points	90.6%
PointNet + Orientation[31]	points	88.6%
DGCNN + Orientation[31]	points	90.7%
PointNet + STRL[20]	points	88.3%
DGCNN + STRL[20]	points	90.9%
PointNet + CrossPoint[1]	points	89.1%
DGCNN + CrossPoint[1]	points	91.2%
STransformer + OcCo[48]	points	89.6%
STransformer + Point-BERT[64]	points	87.4%
3D-OAE(Ours)	points	92.3%

Supervised Fine-tuning In this experiment, we explore the ability of our model to transfer to downstream classification tasks. The **supervised** models are trained from scratch and the **self-supervised** models use the trained weights from self-supervised learning as the initial weights for fine-tuning. All the self-supervised methods use the standard Transformer(STransformer) as backbone architecture. In comparison, our 3D-OAE brings 2.0%(91.4%/93.4%) accuracy improvement over training from scratch. And our method also outperforms PCT [14], which is a variety of standard Transformer. The result proves that using our self-supervised learning scheme, a standard Transformer with no inductive bias could also learn a powerful representation.

Table 2. Shape classification results fine-tuned on ModelNet40

Category	Method	Accuracy
Supervised	PointNet[32]	89.2%
	PointNet++[33]	90.5%
	PointCNN[24]	92.2%
	DGCNN[51]	92.2%
	PCT[14]	93.2%
	STransformer	91.4%
Self-supervised	STransformer + OcCo[48]	92.1%
	STransformer + Point-BERT[64]	93.2%
	3D-OAE(Ours)	93.4%

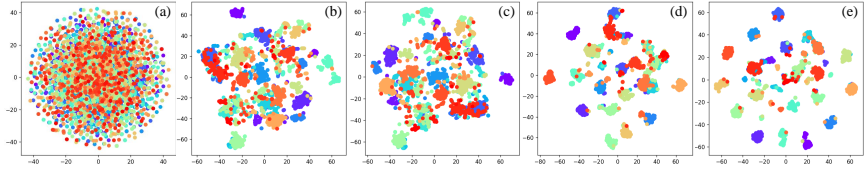


Fig. 4. Visualization of feature distributions. We visualize the features of test sets in ModelNet40 using t-SNE. (a) random initialization, (b) 3D-OAE pre-trained on ShapeNet, (c) Point-BERT pre-trained on ShapeNet, (d) train a randomly initialized encoder on ModelNet40, (e) fine-tuning learned encoder of 3D-OAE on ModelNet40.

Embedding Visualizations We visualize the feature distributions using t-SNE [29]. Fig. 4(b) shows the features learned by 3D-OAE after self-supervised training on the ShapeNet dataset. It’s clear that the feature space of different categories which are mixed together in random initialization(Fig. 4(a)) can be well separated into different regions by 3D-OAE. We also achieve comparable performance with Point-BERT(Fig. 4(c)). As shown in Fig. 4(e), the feature space are almost separated completely independent after fine-tuning on ModelNet40 train sets, and are more clearly disentangled than training from scratch (Fig. 4(d)). It proves that 3D-OAE can guide Transformers to learn powerful representations from unlabelled data, even from different dataset.

Table 3. Few-shot classification results on ModelNet40

	5 way		10 way	
	10-shot	20-shot	10-shot	20-shot
DGCNN-rand	91.8 \pm 3.7	93.4 \pm 3.2	86.3 \pm 6.2	90.9 \pm 5.1
DGCNN-OcCo	91.9 \pm 3.3	93.9 \pm 3.1	86.4 \pm 5.4	91.3 \pm 4.6
STransformer-rand	87.8 \pm 5.2	93.3 \pm 4.3	84.6 \pm 5.5	89.4 \pm 6.3
STransformer-OcCo	94.0 \pm 3.6	95.9 \pm 2.3	89.4 \pm 5.1	92.4 \pm 4.6
STransformer-Point-BERT	94.6 \pm 3.1	96.3 \pm 2.7	91.0 \pm 5.4	92.7 \pm 5.1
3D-OAE	96.3 \pm 2.5	98.2 \pm 1.5	92.0 \pm 5.3	94.6 \pm 3.6

4.3 Few-shot Learning

We further evaluate our model by conducting few-shot learning experiments on ModelNet40. A common used setting is “K-way N-shot”, where K classes are first random selected, and then (N+20) models are sampled from each class. The model is trained on $K \times N$ samples, and evaluated on $K \times 20$ samples. Following previous work [38,64], we choose 4 different few-shot learning settings: “5 way, 10 shot”, “5 way, 20 shot”, “5 way, 10 shot” and “10 way, 20 shot”. For fair comparison, we use the data processed by Point-BERT [64] to conduct 10 separate experiments on each few-shot setting. Table 3 reports the mean accuracy and standard deviation of these 10 runs.

We compare our model with currently state-of-the-art methods OcCo [48] and Point-BERT [64]. As shown in Table 3, using standard Transformer as

Table 4. Part segmentation results on the ShapeNetPart dataset. We report the mean IoU across all instance and IoU for each categories.

Methods	mIoU _I	aero	bag	cap	car	chair	ear.	guitar	knife	lamp	lap.	motor	mug	pistol	rock.	skate.	table
PointNet[32]	83.7	83.4	78.7	82.5	74.9	89.6	73.0	91.5	85.9	80.8	95.3	65.2	93	81.2	57.9	72.8	80.6
PointNet++[33]	85.1	82.4	79	87.7	77.3	90.8	71.8	91	85.9	83.7	95.3	71.6	94.1	81.3	58.7	76.4	82.6
DGCNN[51]	85.2	84	83.4	86.7	77.8	90.6	74.7	91.2	87.5	82.8	95.7	66.3	94.9	81.1	63.5	74.5	82.6
STransformer	85.1	82.9	85.4	87.7	78.8	90.5	80.8	91.1	87.7	85.3	95.6	73.9	94.9	83.5	61.2	74.9	80.6
STransformer-OcCo	85.1	83.3	85.2	88.3	79.9	90.7	74.1	91.9	87.6	84.7	95.4	75.5	94.4	84.1	63.1	75.7	80.8
STransformer-PBert	85.6	84.3	84.8	88.0	79.8	91.0	81.7	91.6	87.9	85.2	95.6	75.6	94.7	84.3	63.4	76.3	81.5
3D-OAE	85.7	83.4	85.0	83.8	79.3	80.1	80.1	91.9	87.2	82.5	95.3	76.0	95.1	85.6	63.5	80.5	83.6

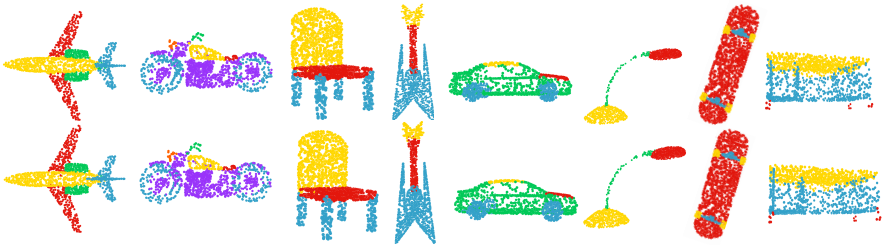


Fig. 5. Visualization of our part segmentation results. Different colors indicate different parts. Top row shows results predicted by our model; bottom row shows corresponding ground truth.

backbone, our purposed 3D-OAE achieves a significant improvement of 8.5%, 4.9%, 7.4%, 5.2% over baseline, and 1.7%, 1.9%, 1.0%, 1.9% over the runner-up method Point-BERT in 4 different sets of few-shot classification. The outstanding performance on few-shot learning proves the strong ability of 3D-OAE to transfer to downstream tasks using very limited data.

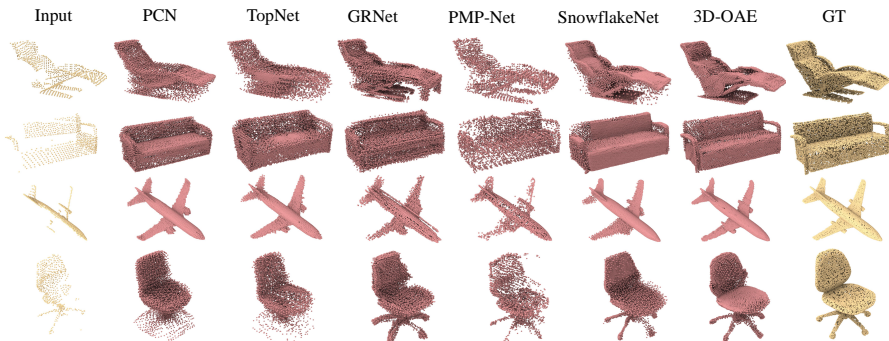
4.4 Object Part Segmentation

Object part segmentation is a challenging task which aims to predict the part label for each point of the model. The ShapeNetPart [62] dataset consists of 16,800 models from 16 categories and is split into 14006/2874 for training and testing. We sample 2048 points from each model follow PointNet [32], and apply a segmentation head achieved by Point-BERT [64] to propagates the group features to each point hierarchically.

As shown in Table 4, our model achieves 0.6% improvement over training a standard Transformer from scratch, while OcCo fails to improve performance. 3D-OAE also outperforms PointNet, PointNet++ and DGCNN. A visualization of our segmentation results is shown in Fig. 5. It's clear that our model is able to make the right predictions at most points, and there are only small visual differences between our predictions and the ground truth.

Table 5. Point cloud completion on PCN dataset. The results is reported in terms of per-point L1 Chamfer distance $\times 10^3$ (lower is better).

Methods	Average	Plane	Cabinet	Car	Chair	Lamp	Couch	Table	Boat
FoldingNet [61]	14.31	9.49	15.80	12.61	15.55	16.41	15.97	13.65	14.99
TopNet [42]	12.15	7.61	13.31	10.90	13.82	14.44	14.78	11.22	11.12
AtlasNet [13]	10.85	6.37	11.94	10.10	12.06	12.37	12.99	10.33	10.61
PCN [65]	9.64	5.50	22.70	10.63	8.70	11.00	11.34	11.68	8.59
GRNet [57]	8.83	6.45	10.37	9.45	9.41	7.96	10.51	8.44	8.04
CDN [50]	8.51	4.79	9.97	8.31	9.49	8.94	10.69	7.81	8.05
PMP-Net [52]	8.73	5.65	11.24	9.64	9.51	6.95	10.83	8.72	7.25
NSFA [68]	8.06	4.76	10.18	8.63	8.53	7.03	10.53	7.35	7.48
PoinTr [63]	8.38	4.75	10.47	8.68	9.39	7.75	10.93	7.78	7.29
SnowflakeNet [56]	7.21	4.29	9.16	8.08	7.89	6.07	9.23	6.55	6.40
STransformer-Scratch	7.37	4.28	9.45	8.21	7.99	6.35	9.38	6.77	6.50
STransformer-OcCo[48]	7.11	4.07	9.16	8.00	7.65	6.08	9.26	6.41	6.27
3D-OAE	6.97	3.99	8.98	7.90	7.46	5.96	8.96	6.31	6.19

**Fig. 6. Visual comparison of point cloud completion on PCN dataset.** The input and ground truth have 2048 and 16384 points, respectively. Compared with current state-of-the-art completion methods like GRNet[57], PMP-Net[52] and SnowflakeNet[56], our 3D-OAE generates more smooth surfaces and more detailed structures.

4.5 Transfer to Generative Tasks

Since most of the previous self-supervised learning methods only focus on the discriminant ability of the representation learned by their model and verify it by transferring the model to classification tasks. They fail to transfer their model to downstream generative tasks(eg. point cloud completion, point cloud up-sampling). In this section, we show the transfer learning ability of 3D-OAE to downstream generative tasks by conducting point cloud completion experiments.

Dataset briefs and evaluation metric. The PCN [65] dataset is one of the most widely used benchmark datasets in point cloud completion task. For a fair comparison, we use the same train/test split settings of PCN[65] and follow previous works to adopt the L1 version of Chamfer distance for evaluation. We use a standard Transformer encoder and a Transformer-based decoder proposed in PoinTr [63] as our backbone, and OcCo is trained using the same architecture.

Table 6. Classification results on the ScanObjectNN dataset.

Methods	OBJ-BG	OBJ-ONLY	PB-T50-RS
PointNet[32]	73.3	79.2	68.0
PointNet++[33]	82.3	84.3	77.9
SpiderCNN[59]	77.1	79.5	73.7
PointCNN[24]	86.1	85.5	78.5
DGCNN[51]	82.8	86.2	78.1
BGA-DGCNN[44]	-	-	79.7
BGA-PointNet++[44]	-	-	80.2
STransformer	79.86	80.55	77.24
STransformer-OcCo[48]	84.85	85.54	78.79
STransformer-PBERT[64]	87.43	88.12	83.07
3D-OAE	89.16	88.64	83.17

Quantitative comparison. The results of our proposed 3D-OAE and other completion methods are shown on Table 5, where 3D-OAE achieves the state-of-the-art performance over all counterparts compared with both supervised and self-supervised methods. We found that 3D-OAE reduces the average CD by 0.4 compared with training a standard Transformer from scratch. Especially, 3D-OAE with only a standard Transformer-based model reduces the average CD by 0.24 compared with the state-of-the-art supervised method SnowflakeNet [56] which proposed a carefully designed model to improve the performance on point cloud completion task. And 3D-OAE also reduces the average CD by 0.14 compared with the state-of-the-art self-supervised method OcCo [48] which also takes a generation task to learn the self-supervised representation. These results prove that our generative self-supervised learning framework is able to learn a powerful representation which can bring significant improvement in downstream generative tasks, we may find a way to avoid spending lots of efforts on designing complex and heavy network structures. It’s also worth noticing that we only use 1024 points during self-supervised learning, but transfer well to PCN dataset where the input has 2048 points. The visual comparisons of point cloud completion on PCN dataset is shown in Fig. 6.

4.6 Transfer to Real-World Data

To further evaluate the representation ability of our method, we use the encoder of 3D-OAE which is trained on the synthetic ShapeNet dataset to fine-tune on a real-world dataset ScanObjectNN. Due to the existence of background, occlusions and noise, this benchmark poses significant challenges to existing methods. We follow previous works to conduct experiments on three main variants: OBJ-BG, OBJ-ONLY and PB-T50-RS.

As shown in Table 6, our proposed 3D-OAE brings significant improvement of 9.03%, 8.09% , 5.93% over training a standard Transformer from scratch, and also outperforms the state-of-the-art methods OcCo and Point-BERT. The strong results show that using our self-supervised framework could learn meaningful

Table 7. Ablation study. We analyze each design of 3D-OAE and report both the Linear SVM and supervised fine-tuning result of ModelNet40.

Methods	Centralize	Loss	Occlusion	Group	Linear Acc.	Fine-t. Acc.
Solution A	✗	CD	Rand	32×64	20.8	–
Solution B	✓	EMD	Rand	32×64	88.4	92.4
Solution C	✓	CD	Block	32×64	91.5	92.7
Solution D	✓	CD	Rand	16×128	91.0	93.0
Solution E	✓	CD	Rand	32×32	91.1	92.5
Solution F	✓	CD	Rand	32×64	92.3	93.4

information from artificial synthetic data and transfer it to real-world data, which could partly solve the domain gap between synthetic and scanned 3D data.

4.7 Ablation study

We analyze the effectiveness of each design in 3D-OAE. For convenience, we conduct all experiments on the ShapeNet dataset, and report the classification accuracy of both Linear SVM and supervised fine-tuning in ModelNet40. By default, all the experiment settings remains the same as Sec. 4.1, except for the analyzed part.

Effect of each design in 3D-OAE. To evaluate the effectiveness of each design in 3D-OAE, we make comparisons between six different experimental solutions shown in Table 7. Solution A is trained without centralizing point patches to seed points. Solution B is trained using Earth Mover’s Distance as the loss function. Solution C is trained with a block occlusion strategy. Solution D is trained with a grouping strategy of 16×128. Solution E is trained with a grouping strategy of 32×32. And Solution F is our default setting. It’s clear that all the purposed designs in 3D-OAE can improve the performance of our method. And we find that using patch mix strategy [66,67] fails to enhance the representation learning ability of 3D-OAE.

Occluding ratio. Table 8 shows the numerical comparison of different occlusion ratios. Similar to MAE [17], we find that the occlusion ratio of 75% performs the best on both the linear accuracy and supervised

Table 8. Ablation study on occlusion ratios.

Occlusion ratio	Linear Acc.	Fine-t. Acc.
0.5	90.9	93.1
0.65	91.1	92.7
0.75	92.3	93.4
0.85	90.7	93.0

fine-tuning accuracy. This is very different from BERT-style self-supervised learning works, where BRET masks only 15% of words and Point-BERT choose to occlude 25% to 45% of the point patches.

5 Conclusion

In this paper, we present a novel point cloud self-supervised learning framework, named 3D Occlusion Auto-Encoder (3D-OAE). Our method shows powerful ability on transferring the learned representations to various downstream tasks, even to generative tasks and real-world tasks. Specifically, we conduct comprehensive experiments on six different downstream tasks, and achieves SOTA performance in each task. These results show that predicting complete shapes from highly occluded ones is an effective way for self-supervised representation learning for point clouds. Moreover, 3D-OAE also shows great efficiency since our encoder only operates on 25% of the input point cloud patches.

References

1. Afham, M., Dissanayake, I., Dissanayake, D., Dharmasiri, A., Thilakarathna, K., Rodrigo, R.: CrossPoint: Self-supervised cross-modal contrastive learning for 3D point cloud Understanding. arXiv preprint arXiv:2203.00680 (2022)
2. Alexiou, E., Upenik, E., Ebrahimi, T.: Towards subjective quality assessment of point cloud imaging in augmented reality. In: 2017 IEEE 19th International Workshop on Multimedia Signal Processing (MMSP). pp. 1–6. IEEE (2017)
3. Bao, H., Dong, L., Wei, F.: Beit: Bert pre-training of image transformers. arXiv preprint arXiv:2106.08254 (2021)
4. Brown, T., Mann, B., Ryder, N., Subbiah, M., Kaplan, J.D., Dhariwal, P., Neelakantan, A., Shyam, P., Sastry, G., Askell, A., et al.: Language models are few-shot learners. *Advances in Neural Information Processing Systems* **33**, 1877–1901 (2020)
5. Carion, N., Massa, F., Synnaeve, G., Usunier, N., Kirillov, A., Zagoruyko, S.: End-to-end object detection with transformers. In: *Proceedings of the European Conference on Computer Vision*. pp. 213–229. Springer (2020)
6. Chang, A.X., Funkhouser, T., Guibas, L., Hanrahan, P., Huang, Q., Li, Z., Savarese, S., Savva, M., Song, S., Su, H., et al.: ShapeNet: An information-rich 3D model repository. arXiv preprint arXiv:1512.03012 (2015)
7. Chen, M., Radford, A., Child, R., Wu, J., Jun, H., Luan, D., Sutskever, I.: Generative pretraining from pixels. In: *International Conference on Machine Learning*. pp. 1691–1703. PMLR (2020)
8. Cui, Y., Chen, R., Chu, W., Chen, L., Tian, D., Li, Y., Cao, D.: Deep learning for image and point cloud fusion in autonomous driving: A review. *IEEE Transactions on Intelligent Transportation Systems* (2021)
9. Devlin, J., Chang, M.W., Lee, K., Toutanova, K.: Bert: Pre-training of deep bidirectional transformers for language understanding. arXiv preprint arXiv:1810.04805 (2018)
10. Dosovitskiy, A., Beyer, L., Kolesnikov, A., Weissenborn, D., Zhai, X., Unterthiner, T., Dehghani, M., Minderer, M., Heigold, G., Gelly, S., et al.: An image is worth 16x16 words: Transformers for image recognition at scale. arXiv preprint arXiv:2010.11929 (2020)
11. Eckart, B., Yuan, W., Liu, C., Kautz, J.: Self-supervised learning on 3D point clouds by learning discrete generative models. In: *Proceedings of the IEEE/CVF Conference on Computer Vision and Pattern Recognition*. pp. 8248–8257 (2021)
12. Gadelha, M., Wang, R., Maji, S.: Multiresolution tree networks for 3D point cloud processing. In: *Proceedings of the European Conference on Computer Vision*. pp. 103–118 (2018)
13. Groueix, T., Fisher, M., Kim, V.G., Russell, B.C., Aubry, M.: A papier-mâché approach to learning 3D surface generation. In: *Proceedings of the IEEE/CVF Conference on Computer Vision and Pattern Recognition*. pp. 216–224 (2018)
14. Guo, M.H., Cai, J.X., Liu, Z.N., Mu, T.J., Martin, R.R., Hu, S.M.: PCT: Point cloud transformer. *Computational Visual Media* **7**(2), 187–199 (2021)
15. Han, Z., Shang, M., Liu, Y.S., Zwicker, M.: View inter-prediction GAN: Unsupervised representation learning for 3D shapes by learning global shape memories to support local view predictions. In: *Proceedings of the AAAI Conference on Artificial Intelligence*. vol. 33, pp. 8376–8384 (2019)
16. Han, Z., Wang, X., Liu, Y.S., Zwicker, M.: Multi-Angle Point Cloud-VAE: Unsupervised feature learning for 3D point clouds from multiple angles by joint self-reconstruction and half-to-half prediction. In: *Proceedings of the IEEE/CVF International Conference on Computer Vision*. pp. 10441–10450. IEEE (2019)

17. He, K., Chen, X., Xie, S., Li, Y., Dollár, P., Girshick, R.: Masked autoencoders are scalable vision learners. arXiv preprint arXiv:2111.06377 (2021)
18. Hu, Q., Yang, B., Xie, L., Rosa, S., Guo, Y., Wang, Z., Trigoni, N., Markham, A.: Randla-net: Efficient semantic segmentation of large-scale point clouds. In: Proceedings of the IEEE/CVF Conference on Computer Vision and Pattern Recognition. pp. 11108–11117 (2020)
19. Hua, B.S., Tran, M.K., Yeung, S.K.: Pointwise convolutional neural networks. In: Proceedings of the IEEE/CVF Conference on Computer Vision and Pattern Recognition. pp. 984–993 (2018)
20. Huang, S., Xie, Y., Zhu, S.C., Zhu, Y.: Spatio-temporal self-supervised representation learning for 3D point clouds. In: Proceedings of the IEEE/CVF International Conference on Computer Vision. pp. 6535–6545 (2021)
21. Joshi, M., Chen, D., Liu, Y., Weld, D.S., Zettlemoyer, L., Levy, O.: Spanbert: Improving pre-training by representing and predicting spans. Transactions of the Association for Computational Linguistics **8**, 64–77 (2020)
22. Khan, S., Naseer, M., Hayat, M., Zamir, S.W., Khan, F.S., Shah, M.: Transformers in vision: A survey. ACM Computing Surveys (CSUR) (2021)
23. Li, J., Chen, B.M., Lee, G.H.: So-net: Self-organizing network for point cloud analysis. In: Proceedings of the IEEE/CVF Conference on Computer Vision and Pattern Recognition. pp. 9397–9406 (2018)
24. Li, Y., Bu, R., Sun, M., Wu, W., Di, X., Chen, B.: Pointcnn: Convolution on x-transformed points. Advances in Neural Information Processing Systems **31** (2018)
25. Liu, X., Han, Z., Wen, X., Liu, Y.S., Zwicker, M.: L2g auto-encoder: Understanding point clouds by local-to-global reconstruction with hierarchical self-attention. In: Proceedings of the 27th ACM International Conference on Multimedia. pp. 989–997 (2019)
26. Liu, Y., Ott, M., Goyal, N., Du, J., Joshi, M., Chen, D., Levy, O., Lewis, M., Zettlemoyer, L., Stoyanov, V.: Roberta: A robustly optimized bert pretraining approach. arXiv preprint arXiv:1907.11692 (2019)
27. Liu, Z., Lin, Y., Cao, Y., Hu, H., Wei, Y., Zhang, Z., Lin, S., Guo, B.: Swin transformer: Hierarchical vision transformer using shifted windows. In: Proceedings of the IEEE/CVF International Conference on Computer Vision. pp. 10012–10022 (2021)
28. Loshchilov, I., Hutter, F.: Decoupled weight decay regularization. arXiv preprint arXiv:1711.05101 (2017)
29. Van der Maaten, L., Hinton, G.: Visualizing data using t-sne. Journal of machine learning research **9**(11) (2008)
30. Pomerleau, F., Colas, F., Siegwart, R.: A review of point cloud registration algorithms for mobile robotics. Foundations and Trends in Robotics **4**(1), 1–104 (2015)
31. Poursaeed, O., Jiang, T., Qiao, H., Xu, N., Kim, V.G.: Self-supervised learning of point clouds via orientation estimation. In: 2020 International Conference on 3D Vision (3DV). pp. 1018–1028. IEEE (2020)
32. Qi, C.R., Su, H., Mo, K., Guibas, L.J.: PointNet: Deep learning on point sets for 3D classification and segmentation. In: Proceedings of the IEEE/CVF Conference on Computer Vision and Pattern Recognition. pp. 652–660 (2017)
33. Qi, C.R., Yi, L., Su, H., Guibas, L.J.: Pointnet++: Deep hierarchical feature learning on point sets in a metric space. Advances in neural information processing systems **30** (2017)
34. Radford, A., Wu, J.: Rewon child, david luan, dario amodei, and ilya sutskever. 2019. Language models are unsupervised multitask learners. OpenAI Blog **1**(8), 9 (2019)

35. Rao, Y., Lu, J., Zhou, J.: Global-local bidirectional reasoning for unsupervised representation learning of 3D point clouds. In: Proceedings of the IEEE/CVF Conference on Computer Vision and Pattern Recognition. pp. 5376–5385 (2020)
36. Sanghi, A.: Info3D: Representation learning on 3D objects using mutual information maximization and contrastive learning. In: Proceedings of the European Conference on Computer Vision. pp. 626–642. Springer (2020)
37. Sauder, J., Sievers, B.: Self-supervised deep learning on point clouds by reconstructing space. *Advances in Neural Information Processing Systems* **32** (2019)
38. Sharma, C., Kaul, M.: Self-supervised few-shot learning on point clouds. *Advances in Neural Information Processing Systems* **33**, 7212–7221 (2020)
39. Shen, Y., Feng, C., Yang, Y., Tian, D.: Mining point cloud local structures by kernel correlation and graph pooling. In: Proceedings of the IEEE/CVF Conference on Computer Vision and Pattern Recognition. pp. 4548–4557 (2018)
40. Su, H., Jampani, V., Sun, D., Maji, S., Kalogerakis, E., Yang, M.H., Kautz, J.: Splatnet: Sparse lattice networks for point cloud processing. In: Proceedings of the IEEE/CVF Conference on Computer Vision and Pattern Recognition. pp. 2530–2539 (2018)
41. Sun, C., Zheng, Z., Wang, X., Xu, M., Yang, Y.: Point cloud pre-training by mixing and disentangling. *arXiv preprint arXiv:2109.00452* (2021)
42. Tchapmi, L.P., Kosaraju, V., Rezaatofghi, H., Reid, I., Savarese, S.: TopNet: Structural point cloud decoder. In: Proceedings of the IEEE/CVF Conference on Computer Vision and Pattern Recognition. pp. 383–392 (2019)
43. Thomas, H., Qi, C.R., Deschard, J.E., Marcotegui, B., Goulette, F., Guibas, L.J.: Kpconv: Flexible and deformable convolution for point clouds. In: Proceedings of the IEEE/CVF international conference on computer vision. pp. 6411–6420 (2019)
44. Uy, M.A., Pham, Q.H., Hua, B.S., Nguyen, T., Yeung, S.K.: Revisiting point cloud classification: A new benchmark dataset and classification model on real-world data. In: Proceedings of the IEEE/CVF International Conference on Computer Vision. pp. 1588–1597 (2019)
45. Valsesia, D., Fracastoro, G., Magli, E.: Learning localized representations of point clouds with graph-convolutional generative adversarial networks. *IEEE Transactions on Multimedia* **23**, 402–414 (2020)
46. Vaswani, A., Shazeer, N., Parmar, N., Uszkoreit, J., Jones, L., Gomez, A.N., Kaiser, L., Polosukhin, I.: Attention is all you need. *Advances in Neural Information Processing Systems* **30** (2017)
47. Verma, N., Boyer, E., Verbeek, J.: Feastnet: Feature-steered graph convolutions for 3D shape analysis. In: Proceedings of the IEEE/CVF Conference on Computer Vision and Pattern Recognition. pp. 2598–2606 (2018)
48. Wang, H., Liu, Q., Yue, X., Lasenby, J., Kusner, M.J.: Unsupervised point cloud pre-training via occlusion completion. In: Proceedings of the IEEE/CVF International Conference on Computer Vision. pp. 9782–9792 (2021)
49. Wang, L., Huang, Y., Hou, Y., Zhang, S., Shan, J.: Graph attention convolution for point cloud semantic segmentation. In: Proceedings of the IEEE/CVF Conference on Computer Vision and Pattern Recognition. pp. 10296–10305 (2019)
50. Wang, X., Ang Jr, M.H., Lee, G.H.: Cascaded refinement network for point cloud completion. In: Proceedings of the IEEE/CVF Conference on Computer Vision and Pattern Recognition. pp. 790–799 (2020)
51. Wang, Y., Sun, Y., Liu, Z., Sarma, S.E., Bronstein, M.M., Solomon, J.M.: Dynamic graph cnn for learning on point clouds. *Acm Transactions On Graphics (ToG)* **38**(5), 1–12 (2019)

52. Wen, X., Xiang, P., Han, Z., Cao, Y.P., Wan, P., Zheng, W., Liu, Y.S.: PMP-Net: Point cloud completion by learning multi-step point moving paths. In: Proceedings of the IEEE/CVF Conference on Computer Vision and Pattern Recognition. pp. 7443–7452 (2021)
53. Wu, J., Zhang, C., Xue, T., Freeman, B., Tenenbaum, J.: Learning a probabilistic latent space of object shapes via 3D generative-adversarial modeling. *Advances in Neural Information Processing Systems* **29** (2016)
54. Wu, W., Qi, Z., Fuxin, L.: PointConv: Deep convolutional networks on 3D point clouds. In: Proceedings of the IEEE/CVF Conference on Computer Vision and Pattern Recognition. pp. 9621–9630 (2019)
55. Wu, Z., Song, S., Khosla, A., Yu, F., Zhang, L., Tang, X., Xiao, J.: 3D ShapeNets: A deep representation for volumetric shapes. In: Proceedings of the IEEE/CVF Conference on Computer Vision and Pattern Recognition. pp. 1912–1920 (2015)
56. Xiang, P., Wen, X., Liu, Y.S., Cao, Y.P., Wan, P., Zheng, W., Han, Z.: SnowflakeNet: Point cloud completion by snowflake point deconvolution with skip-transformer. In: Proceedings of the IEEE/CVF International Conference on Computer Vision. pp. 5499–5509 (2021)
57. Xie, H., Yao, H., Zhou, S., Mao, J., Zhang, S., Sun, W.: Grnet: Gridding residual network for dense point cloud completion. In: Proceedings of the European Conference on Computer Vision. pp. 365–381. Springer (2020)
58. Xie, S., Gu, J., Guo, D., Qi, C.R., Guibas, L., Litany, O.: PointContrast: Un-supervised pre-training for 3D point cloud understanding. In: Proceedings of the European Conference on Computer Vision. pp. 574–591. Springer (2020)
59. Xu, Y., Fan, T., Xu, M., Zeng, L., Qiao, Y.: Spidercnn: Deep learning on point sets with parameterized convolutional filters. In: Proceedings of the European Conference on Computer Vision. pp. 87–102 (2018)
60. Yang, J., Zhang, Q., Ni, B., Li, L., Liu, J., Zhou, M., Tian, Q.: Modeling point clouds with self-attention and gumbel subset sampling. In: Proceedings of the IEEE/CVF Conference on Computer Vision and Pattern Recognition. pp. 3323–3332 (2019)
61. Yang, Y., Feng, C., Shen, Y., Tian, D.: Foldingnet: Point cloud auto-encoder via deep grid deformation. In: Proceedings of the IEEE/CVF Conference on Computer Vision and Pattern Recognition. pp. 206–215 (2018)
62. Yi, L., Kim, V.G., Ceylan, D., Shen, I.C., Yan, M., Su, H., Lu, C., Huang, Q., Sheffer, A., Guibas, L.: A scalable active framework for region annotation in 3D shape collections. *ACM Transactions on Graphics (ToG)* **35**(6), 1–12 (2016)
63. Yu, X., Rao, Y., Wang, Z., Liu, Z., Lu, J., Zhou, J.: PoinTr: Diverse point cloud completion with geometry-aware transformers. In: Proceedings of the IEEE/CVF International Conference on Computer Vision. pp. 12498–12507 (2021)
64. Yu, X., Tang, L., Rao, Y., Huang, T., Zhou, J., Lu, J.: Point-BERT: Pre-training 3D point cloud transformers with masked point modeling. In: Proceedings of the IEEE Conference on Computer Vision and Pattern Recognition (CVPR) (2022)
65. Yuan, W., Khot, T., Held, D., Mertz, C., Hebert, M.: Pcn: Point completion network. In: 2018 International Conference on 3D Vision (3DV). pp. 728–737. IEEE (2018)
66. Yun, S., Han, D., Oh, S.J., Chun, S., Choe, J., Yoo, Y.: Cutmix: Regularization strategy to train strong classifiers with localizable features. In: Proceedings of the IEEE/CVF International Conference on Computer Vision. pp. 6023–6032 (2019)
67. Zhang, J., Chen, L., Ouyang, B., Liu, B., Zhu, J., Chen, Y., Meng, Y., Wu, D.: Pointcutmix: Regularization strategy for point cloud classification. *arXiv preprint arXiv:2101.01461* (2021)

68. Zhang, W., Yan, Q., Xiao, C.: Detail preserved point cloud completion via separated feature aggregation. In: Proceedings of the European Conference on Computer Vision. pp. 512–528. Springer (2020)
69. Zhang, Z., Girdhar, R., Joulin, A., Misra, I.: Self-supervised pretraining of 3D features on any point-cloud. In: Proceedings of the IEEE/CVF International Conference on Computer Vision. pp. 10252–10263 (2021)
70. Zhang, Z., Hua, B.S., Yeung, S.K.: Shellnet: Efficient point cloud convolutional neural networks using concentric shells statistics. In: Proceedings of the IEEE/CVF International Conference on Computer Vision. pp. 1607–1616 (2019)
71. Zhao, H., Jiang, L., Jia, J., Torr, P.H., Koltun, V.: Point transformer. In: Proceedings of the IEEE/CVF International Conference on Computer Vision. pp. 16259–16268 (2021)
72. Zhao, Y., Birdal, T., Deng, H., Tombari, F.: 3D point capsule networks. In: Proceedings of the IEEE/CVF Conference on Computer Vision and Pattern Recognition. pp. 1009–1018 (2019)